Geometric and dielectric characterization of porous media

R. Hilfer
Department of Physics, University of Oslo, 0316 Oslo, Norway,
and Institut für Physik,
Universität Mainz, 6500 Mainz, Germany
(Received 12 October 1990)

This paper introduces local porosity distributions and local percolation probabilities as well-defined and experimentally observable geometric characteristics of general porous media. Based on these concepts the dielectric response is analyzed using the effective-medium approximation and percolation scaling theory. The theoretical origin of static and dynamic scaling laws for the dielectric response including Archie's law in the low-porosity limit are elucidated. The zero-frequency real dielectric constant is found to diverge as $\epsilon'(0) \propto (1-\phi)^{-m'}$ in the high-porosity limit, where ϕ denotes the porosity and m' is analogous to the cementation exponent. Model calculations are presented for the interplay between geometric characteristics and the frequency-dependent dielectric response. Three purely geometric mechanisms are identified, each of which can give rise to a large dielectric enhancement.

I. INTRODUCTION

A long-standing problem of considerable scientific and technological importance is to improve the understanding of geometric-dielectric correlations in porous materials. The scientific problem is to find out which properties of the complicated random geometry of the pore space have a significant influence on the electrical and dielectric properties. The engineer, on the other hand, is interested in the inverse problem of how to infer geometrical features of the porous medium from its dielectric response. The most prominent example for the technological importance of this question arises in the context of well-log interpretation for petroleum or water exploration.[1]

My objective in this paper is to present a simple theoretical framework which allows a systematic study of how the pore-space geometry of an insulating porous material influences the low-frequency dielectric response when the pore space is filled with a conductor. The approach is based on a novel geometric characterization of porous media via local porosity distributions and local percolation probabilities which will be defined in Sec. II. These geometric quantities are conceptually well defined and experimentally observable. The dielectric properties will be calculated directly from the geometric characteristics using mean-field theory, scaling theory, and numerical techniques. The results are intended to be applicable to the physics of water- or brine-saturated clay-free rocks. Such rocks can have very large relative dielectric permittivities, sometimes exceeding those of the constituent materials by a factor of 10^3 or more.[1-5] As a second hallmark for the dielectric response of water-saturated rocks, many investigators report a power-law behavior for the dc conductivity with porosity known as Archie's law.[6] Holwech and Nøst[7] have recently measured the frequency-dependent response of water-filled sintered glass beads and showed that strong dielectric dispersion and Archie's law can arise as a purely geometrical effect.[8] It will be assumed throughout this paper that electrochemical effects are absent.

Despite numerous efforts,[9] no theoretical framework has been found to date which encompasses both aspects, strong dielectric enhancement and Archie's law, simultaneously. Recent theoretical approaches can be divided into two categories: The first class[10-17] attempts to calculate the dielectric properties starting from highly simplified or indirect geometric models for the pore space. The difficulty is that most models are too idealized to be compared even to the simplest experimental model system. The second category[18-23] does not attempt to incorporate the pore-space geometry, but concentrates instead on a sometimes sophisticated phenomenological approach.

Geometrical theories fall again into two families: percolation theories[10-12] and grain mixture models.[13-16] Percolation theories predict a finite porosity below which the conductivity vanishes. Such models are attractive because they capture to some extent the geometry of a random network of pores, and they give rise to a strong dielectric enhancement near the percolation threshold. However, they have been ruled out by the argument[13] that the pore spaces of realistic systems appear to remain connected down to zero porosity (Archie's law). In addition, strong dielectric enhancement does not appear to be correlated with a particular porosity threshold. Grain mixture models, on the other hand, concentrate on the connectedness of the pore space. They are attractive because they incorporate to some extent the consolidation processes though which porous rocks are formed. Similar to abstract resistor network models,[10] they are usually not very explicit about the microgeometry underlying a specific model. While predicting grain-shape-dependent

exponents for Archie's law the grain mixture models need to assume the presence of strongly platelike grains to obtain dielectric enhancement. It was pointed out by Wong, Koplik, and Tomanic[17] however, that the cementation index in Archie's law is not determined by grain shape. On the experimental side, it was concluded[5] for the case of White stone that the spheroidal grain model cannot account simultaneously for the observed frequency-dependent conductivity and dielectric constant.

Let me conclude the brief discussion of recent theories with phenomenological approaches which form the second large category. Most approaches[18–21] are based on the spectral representation of the complex dielectric functions developed by Fuchs[22] and Bergman.[23] These theories start from an abstract pole spectrum which can be adjusted to reproduce the features of experimental data.[6] Unfortunately, the pole spectrum or its properties cannot be related to the pore-space geometry without prior geometric modeling. Therefore, the theory by itself, while separating material and geometric aspects, does not lead to a better understanding of geometric-dielectric correlations in porous media.

To develop a better understanding of geometric-dielectric correlations in porous media, it is first necessary to develop a suitable geometric characterization as a starting point. Instead of considering the different "sizes" of pores as the fundamental source of randomness in porous media, the present approach suggests to consider the porosity itself as the fundamental random variable. This leads immediately to suggest local porosity distributions and local percolation probabilities as partial geometric characterizations of the complex pore space.

Based on these new geometric characterizations, the following questions will be discussed in this paper: validity and theoretical origin of static and dynamic scaling laws, including Archie's law, and the universality of scaling indices (Sec. V), geometric mechanisms of dielectric enhancement (Sec. VI), model calculations for the interplay between geometric characteristics and frequency-dependent dielectric response (Sec. VI), and theoretical aspects of how to obtain geometric information from the dielectric response (Sec. VII). It must be emphasized again that dielectric dispersion in this paper results only from the randomness in the pore-space geometry. In particular, electrochemical effects, which are important in real rocks, are not considered. The dielectric response is found to be surprisingly sensitive to the geometrical features encapsuled in local porosity distributions, and it is hoped that the present investigation might be a step towards developing ultimately a "dielectric spectroscopy" of porous media.

II. GEOMETRIC CHARACTERIZATION OF POROUS MEDIA

The porosity ϕ of a porous medium is defined as the volume of pore space divided by the total volume. The complement of the pore space will be called the matrix. The porosity is the most important geometrical quantity characterizing a porous medium. Clearly, ϕ alone, being just a single number, cannot suffice to characterize the complex pore-space geometry. On the other hand, a complete equivalence class of atlantes for the pore-space boundary considered as a two-dimensional continuous manifold contains too much (possibly irrelevant) geometrical information. Similar to many instances in statistical physics, the task is to find a suitable distribution function such that a finite number of its moments give a faithful approximate representation of the system.

It is often suggested to use a "pore-size distribution" as a possible geometric characterization for porous media, and mercury injection is suggested to measure it. Already Scheidegger,[24] however, pointed out that the pore-size distribution is mathematically ill defined. It depends on an arbitrary identification of cylindrical pores and their diameters.[25] It is now well appreciated[26] that the result of a mercury injection measurement cannot be interpreted without having already a faithful geometrical model of the pore space, which itself requires knowledge of the pore-size distribution. Without such a model, no reliable geometrical information such as the pore-size distribution can be extracted from the measurement.

This paper suggests a different characterization of porous media. Purely geometric quantities will be introduced which are well defined and readily accessible to direct measurement. The characterization is based on viewing the local geometry on a mesoscopic scale as the fundamental random quantity. To define "local geometries," consider a porous medium with a homogeneously and isotropically disordered pore space. The points of a Bravais lattice (in practice a simple cubic lattice) are superimposed on the porous medium and an arbitrary (in practice cubic) primitive cell is chosen. The local geometry around the lattice point $\mathbf{R}$ is defined as the intersection of the pore space and the primitive cell at $\mathbf{R}$. The volume of the primitive (or measurement) cells is $V_{\mathrm{MC}}=1/\rho$, where ρ is the density of Bravais lattice points. This defines the length scale of resolution L as $L=\rho^{-1/3}=(V_{\mathrm{MC}})^{1/3}$. For the simple cubic lattice with cubic primitive cell, L is the lattice constant. The preceding definition of local geometries is valid for topologically and continuously disordered pore spaces. For a porous medium with substitutional disorder, the measurement lattice is given by the underlying lattice.

The local geometry inside the measurement cell will become increasingly complex as the length scale of resolution L is increased. A full geometric characterization at arbitrary L is difficult. However, at every L the local geometry may be partially characterized by two simple properties. One is the cell porosity; the second is whether the pore space percolates or not.

Consider first the local (or cell) porosity. To define it, the characteristic function (indicator function) of an arbitrary set A is introduced as

$$\chi_A(\mathbf{r})=\begin{cases}0 & \text{if } \mathbf{r} \text{ lies outside the set } A\\ 1 & \text{if } \mathbf{r} \text{ lies inside the set } A\end{cases}. \tag{2.1}$$

The local (or cell) porosity $\phi(\mathbf{R},L)$ at the lattice position $\mathbf{R}$ and length scale L is defined as

$$\phi(\mathbf{R},L)=\rho\int\chi_{\mathrm{MC}}(\mathbf{r};\mathbf{R},L)\chi_{\mathrm{PS}}(\mathbf{r})d\mathbf{r}\ , \tag{2.2}$$

where $\chi_{\mathrm{MC}}(\mathbf{r};\mathbf{R},L)$ is the characteristic function of the measurement cell at $\mathbf{R}$ having size L, $\chi_{\mathrm{PS}}(\mathbf{r})$ is the characteristic function of the pore space and the integration extends over the porous medium. One can now define local porosity distribution functions in analogy to atomic distribution functions. Thus $\mu(\phi,\mathbf{R};L)$ measures the probability density to find the local porosity ϕ in the range from ϕ to $\phi+d\phi$ in a cell of linear dimension L at the point $\mathbf{R}$. The assumption of homogeneity implies that $\mu(\phi,\mathbf{R};L)=\mu(\phi;L)$ must be independent of $\mathbf{R}$. The function $\mu(\phi;L)$ will be called the local porosity density at scale L. The bulk porosity $\bar{\phi}$ can be thought of as the integral over a large volume or as the average over a statistical ensemble of measurement cells, and thus, assuming "ergodicity,"

$$\bar{\phi}=\phi(\mathbf{R},L\to\infty)=\int_0^1\phi\mu(\phi;L)d\phi\ , \tag{2.3}$$

independent of $\mathbf{R}$ and L. Higher-order distribution functions can be defined similarly. The n-cell local porosity distribution function $\mu_n(\phi_1,\mathbf{R}_1;\phi_2,\mathbf{R}_2;\ldots;\phi_n,\mathbf{R}_n;L)$ at scale L measures the probability density to find ϕ_1 in the cell at $\mathbf{R}_1$, ϕ_2 in the cell at $\mathbf{R}_2$, etc. The full information about the statistical properties of the porosity distribution at scale L is contained in the local porosity probability functional $\mu\{\phi,L\}$ at scale L which is obtained as the limit $n\to\infty$ of μ_n.

The local porosity distribution $\mu(\phi;L)$ depends strongly on L. There are two competing effects. At small L the local geometries are simple, but they are highly correlated with each other, and the one-cell function $\mu(\phi;L)$ does not contain these complex geometric correlations. At large L the local geometries are statistically uncorrelated, but each one of them is nearly as complex as the geometry of the full pore space. There must then exist an intermediate length scale ξ at which, on the one hand, the local geometries are relatively simple, and on the other hand the single-cell distribution function has sufficient nontrivial geometric content to be a good first approximation. In this paper this length will be taken as a length of the order of the characteristic pore or grain size of the porous medium. More precisely, ξ is determined from the two-cell distribution function $\mu_2(\phi_1,\mathbf{R}_1;\phi_2,\mathbf{R}_2;L)$. The assumption of isotropy implies that the two-cell distribution function depends only on the distance R, i.e.,

$$\mu_2(\phi_1,\mathbf{R}_1;\phi_2,\mathbf{R}_2;L)=\mu_2(\phi_1,\phi_2;R;L)\ . \tag{2.4}$$

The porosity autocorrelation function at scale L is defined as

$$C(R,L)=\frac{\int_0^1\int_0^1(\phi_1-\bar{\phi})(\phi_2-\bar{\phi})\mu_2(\phi_1,\phi_2;R;L)d\phi_1 d\phi_2}{\int_0^1(\phi-\bar{\phi})^2\mu(\phi;R;L)d\phi}\ , \tag{2.5}$$

and the porosity correlation length ξ is obtained from $C(R,L)$ as

$$\xi^2=\frac{\int R^2C(R,0)d^3R}{\int C(R,0)d^3R}\ . \tag{2.6}$$

In the following *the* "local porosity distribution" is defined as $\mu(\phi)=\mu(\phi;\xi)$, the single-cell local porosity density at scale ξ. Simultaneously with this convention it will be assumed that the local geometries at scale ξ are "simple." This is called the "hypothesis of local simplicity," and it will be made more precise in Sec. IV. For systems with an underlying lattice symmetry, the length ξ has to be replaced by the lattice constant.

The most important aspect of $\mu(\phi)=\mu(\phi;\xi)$ is that it is readily measurable using modern image-processing equipment. In the following a simplified and approximate procedure to observe $\mu(\phi)$ in homogeneous and isotropic porous media is discussed. This procedure measures $\mu(\phi)$ from photographs of two-dimensional thin sections through the pore space. These photographs must be colored such that pore space and matrix are clearly distinguished. The quality of the pore-space visualization should be such that a high-resolution digitization of the image allows each pixel to be assigned unambiguously to either pore space or matrix. An approximate correlation length might be calculated by noting that $\lim_{L\to 0}\phi(\mathbf{R},L)$ corresponds to the pixel value 0 or 1, according to whether the pixel at position $\mathbf{R}$ falls into matrix (0) or pore space (1). The porosity autocorrelation function $C(R,0)$ can be calculated from the pixel power spectrum using the Wiener-Khintchine theorem, and the correlation length ξ is obtained from $C(R,0)$ using Eq. (2.6). Having determined the correlation length, the photograph is subdivided into cells by placing, e.g., a square grid with squares of length ξ over it. The cell porosities are then

$$\phi_i=\frac{1}{\xi^2}\sum_{j=1}^{\xi^2}\phi_i(\mathbf{R}_j)\ , \tag{2.7}$$

where $\phi_i(\mathbf{R}_j)$ is the pixel at position $\mathbf{R}_j$ within cell i. The resulting probability density is averaged over different ways of placing the measurement lattice, over many choices of the primitive cell, and over all available photographs of two-dimensional sections to obtain the local porosity density $\mu(\phi)$.

The result of the measuring procedure described in the preceding paragraph will in general lead to a local porosity distribution of the form

$$\mu(\phi)=\mu_0\delta(\phi)+(1-\mu_0-\mu_1)\tilde{\mu}(\phi)+\mu_1\delta(\phi-1) . \quad (2.8)$$

Its bulk (average) porosity $\bar{\phi}$ is obtained as the expectation value $\bar{\phi}=\int_0^1\phi\mu(\phi)d\phi$, in agreement with Eq. (2.3). The local porosity distribution $\mu(\phi)$ contains very much geometrical information about the pore-space geometry. Its definition as $\mu(\phi;\xi)$ is optimal in the sense that it contains the maximum amount of information based purely on the porosity concept. If the cells were chosen much larger than ξ, then the simple form

$$\mu(\phi;L\gg\xi)=\delta(\phi-\bar{\phi}) \quad (2.9)$$

is expected to result. The geometric information in this case is reduced to $\bar{\phi}$. At the same time, the local geometries are nearly as complex as the bulk geometry. If, on the other hand, the cells are chosen very small, i.e., $L\ll\xi$, then the measurement procedure above could still be applied and is expected to yield

$$\mu(\phi;L\ll\xi)=\bar{\phi}\delta(\phi-1)+(1-\bar{\phi})\delta(\phi) . \quad (2.10)$$

Again, the geometrical information in $\mu(\phi)$ is reduced to one number. The geometrical complexity has gone into the correlations between cells contained only in the full porosity probability functional, but not in the single-cell quantity $\mu(\phi)$. In this sense choosing $L\approx\xi$ is optimal.

The local porosity distribution $\mu(\phi)$ is easily calculated for ordered or substitutionally disordered porous media, but very difficult to obtain for topological or continuum disorder. For ordered or substitutionally disordered cases, the measurement is given by the underlying lattice, and ξ is the lattice constant. One finds immediately $\mu(\phi)=\delta(\phi-\bar{\phi})$ for the ordered case, in agreement with Eq. (2.9). For substitutional disorder the local porosity density follows directly from the distribution of the individual geometrical elements which occupy the lattice sites.

The second geometric property to characterize local geometries is whether the pore space percolates or not. For cubic cells each cell is classified as percolating or nonpercolating according to whether or not there exists at least one face of the cube which can be connected to any of the other faces via a path contained completely inside the pore space. For noncubic cells the classification has to be modified appropriately. Let $\lambda(\phi)$ denote the fraction of percolating cells with local porosity ϕ. $\lambda(\phi)$ will be called the "local percolation probability." It is an important geometric quantity for all physical properties of porous media such as conduction or fluid flow because it determines whether volume elements are permeable or not.

The two functions $\mu(\phi)$ and $\lambda(\phi)$ constitute only a partial and approximate geometric characterization of the pore space. However, λ and μ have a rich geometrical content. This becomes obvious from the difficulty of calculating them even for the simplest models of homogeneous and isotropic porous media. At present, no experimentally observed local porosity distributions or percolation probabilities are available to the author.[27] However, I believe that the general shape of $\mu(\phi)$ for pore spaces resulting from spinodal decomposition may be similar to the order-parameter distribution of a two-dimensional Lennard-Jones fluid measured in a recent computer experiment.[28]

III. DIELECTRIC RESPONSE

The low-frequency dielectric response of a porous medium is influenced by the randomness in its pore-space geometry. Given the geometric description of the pore space developed in the last section, two questions arise: One is how the geometrical information encapsuled in $\mu(\phi)$ and $\lambda(\phi)$ expresses itself in the effective complex dielectric constant $\epsilon(\omega)$, where ω is the frequency. This will be called the direct problem. The inverse problem is the question what geometric information can be obtained from a measurement of the frequency-dependent dielectric constant.

To study these two questions, standard effective-medium theory is an appropriate tool for a first approximate investigation. Consider again the subdivision of the porous medium into cells of length ξ. Let ϵ_R and ϵ_W be the complex frequency-dependent dielectric constants of the constituent materials where the index R stands for the rock matrix and the index W stands for water (or brine) filling the pore space. Because all cells are statistically independent, standard one-cell effective-medium theory[29] can be employed to write a self-consistency equation for the effective dielectric constant $\epsilon(\omega)$ of the medium, which reads

$$\int_{\mathcal{G}}\frac{\epsilon_{\rm loc}(\omega;\epsilon_R,\epsilon_W;G)-\epsilon(\omega)}{\epsilon_{\rm loc}(\omega;\epsilon_R,\epsilon_W;G)+2\epsilon(\omega)}d\mu(G)=0 . \quad (3.1)$$

Here $\epsilon_{\rm loc}(\omega;\epsilon_R,\epsilon_W;G)$ is the local effective dielectric constant, which depends on the constituent materials ϵ_R and ϵ_W and the local geometry G. The integration is performed over the space $\mathcal{G}$ of all possible local geometries G, and the probability measure $d\mu(G)$ on $\mathcal{G}$ represents a complete description of the statistical pore-space geometry.

It was discussed in Sec. II that a complete geometric description such as $d\mu(G)$ is not known, and that in the present paper the local porosity distribution $\mu(\phi)$ and the local percolation probability $\lambda(\phi)$ will be used as approximate descriptions. This implies that the local effective dielectric constants $\epsilon_{\rm loc}(\omega;\epsilon_R,\epsilon_W;G)$ must be replaced simultaneously by an approximate effective local dielectric constant $\epsilon(\omega;\phi)$. It depends on the local porosity ϕ as the only geometrical quantity. As a consequence of the basic hypothesis of local simplicity discussed above, $\epsilon(\omega;\phi)$ can later be approximated by simple geometric models of the pore space. Note that the dependence on ϵ_R and ϵ_W as well as the index "loc" have been suppressed to shorten the notation. With these simplifications one arrives at the simpler equation

$$\int_0^1\frac{\epsilon_C(\omega;\phi)-\epsilon(\omega)}{\epsilon_C(\omega;\phi)+2\epsilon(\omega)}\lambda(\phi)\mu(\phi)d\phi + \int_0^1\frac{\epsilon_B(\omega;\phi)-\epsilon(\omega)}{\epsilon_B(\omega;\phi)+2\epsilon(\omega)}[1-\lambda(\phi)]\mu(\phi)d\phi=0 . \quad (3.2)$$

Here $\epsilon_C(\omega;\phi)$ and $\epsilon_B(\omega;\phi)$ are the local effective dielectric constants. The index C stands for conducting (percolating) local geometries and the index B for blocking (nonpercolating) cells.

Equation (3.2) represents the starting point for the present investigation, and it is appropriate to discuss briefly its content. Mathematically, Eq. (3.2) is a complicated integral equation involving five different functions. The average local dielectric properties ϵ_R, ϵ_W are assumed to be known. According to the hypothesis of local simplicity, their precise form is not sensitive to geometric properties other than porosity, and thus they will in practice be determined from very simple geometrical models of the local pore space. The important assumptions implicit in using Eq. (3.2) are twofold: The first is that local geometries are uncorrelated. The second says that the important geometric features giving rise to dielectric dispersion can be described using local porosity distributions and local percolation probabilities. With ϵ_B and ϵ_C known, Eq. (3.2) can be written as $F(\epsilon,\mu,\lambda)=0$. The direct problem is to determine ϵ given λ and μ as geometrical input. The inverse problems are to calculate μ from ϵ and λ or to find λ given ϵ and μ.

Before embarking on the discussion of these problems, some notation and conventions must be established for the subsequent treatment.

IV. NOTATION AND CONVENTIONS

The time variation of electrical fields is taken proportional to $\exp(-i\omega t)$. The complex dielectric constant ϵ is written as

$$\epsilon=\epsilon'+i\epsilon''=\epsilon'+i\frac{\sigma'}{\omega} , \tag{4.1}$$

where ϵ' (ϵ'') are the real (imaginary) parts of ϵ, and σ' is the real part of the complex conductivity σ. SI units will be used. Values for ϵ are given in multiples of $\epsilon_0=8.8542\times10^{-12}$ F/m, the permittivity of free space, and the units for σ' are then S/m. The conductivity is written as

$$\sigma=\sigma'+i\sigma''=\sigma'+i\omega(1-\epsilon') . \tag{4.2}$$

The relationship between σ and ϵ is also written as

$$\epsilon(u)=1-\frac{\sigma(u)}{u} , \tag{4.3}$$

where the notation $u=i\omega$ has been used.

The constituent materials are assumed to be rock forming the matrix and water filling the pore space. Their dielectric constants are

$$\epsilon_W=\epsilon'_W+i\frac{\sigma'_W}{\omega} , \tag{4.4}$$

for water, and

$$\epsilon_R=\epsilon'_R , \tag{4.5}$$

for rock. In calculations the values $\epsilon'_W=79\epsilon_0$ and $\epsilon'_R=7\epsilon_0$ will be used. Dimensionless frequencies are introduced by setting $\omega_0=\sigma'_W/\epsilon'_W=1$ for the relaxation frequency of water, and this also fixes $\epsilon'_W=\sigma'_W$.

The average local dielectric constants $\epsilon_B(\omega;\phi)$ and $\epsilon_C(\omega;\phi)$ at porosity ϕ are in general unknown. Nevertheless, some general statements can be made. The relation

$$\sigma'_B(\omega=0;\phi)=0 \tag{4.6}$$

must hold for all ϕ. It expresses the fact that the blocking geometry is nonconducting. The following relations for the low- and high-porosity limits are also obvious:

$$\sigma'_C(\omega;\phi=0)=\sigma'_R=0 , \tag{4.7a}$$

$$\sigma'_C(\omega;\phi=1)=\sigma'_W , \tag{4.7b}$$

$$\epsilon'_C(\omega;\phi=0)=\epsilon'_B(\omega;\phi=0)=\epsilon'_R , \tag{4.7c}$$

$$\epsilon'_C(\omega;\phi=1)=\epsilon'_B(\omega;\phi=1)=\epsilon'_W , \tag{4.7d}$$

and they are valid for all frequencies ω.

Finally, the local simplicity hypothesis will be cast into mathematical form by requiring that $\sigma'_C(\omega=0;\phi)$ can be expanded for small ϕ as

$$\sigma'_C(0;\phi)=\phi(C_1+C_2\phi+\cdots) . \tag{4.8}$$

Correspondingly, for the blocking geometries the real dielectric constant diverges as $\phi\to1$, which is a thin-plate effect. Local simplicity is assumed to imply that the expansion

$$[\epsilon'_B(0;\phi)]^{-1}=(1-\phi)[B_1+B_2(1-\phi)+\cdots] \tag{4.9}$$

is valid for $\phi<1$. Note that Eq. (4.7d) implies a discontinuity at $\phi=1$.

For the local porosity distribution, it will be assumed that $\mu_0=\mu_1=0$ in Eq. (2.8) and thus $\mu(\phi)=\tilde{\mu}(\phi)$. The local percolation probability has to assume the limiting values

$$\lambda(\phi=0)=0 , \tag{4.10a}$$

$$\lambda(\phi=1)=1 . \tag{4.10b}$$

The first equation states that there are no conducting geometries with porosity 0, and the second says that there exist no blocking geometries at porosity 1.

V. DIRECT PROBLEM

Consider now the direct problem with $\lambda(\phi)$ and $\mu(\phi)$ given. The problem is to calculate $\epsilon(\omega)$. The nonlinear integral equation (3.2) is too difficult for an analytical treatment, and numerical solutions must ultimately be sought. Some analytic information can be obtained, however, by exploiting the similarity to the well-known percolation problem. The analogy arises from the classification of local geometries into percolating and nonpercolating ones. The first question is then whether there indeed exists a percolation threshold.

A. Solution for strongly peaked local porosity distributions

For strongly peaked $\mu(\phi)$, Eq. (3.2) can be expanded around $\bar{\phi}$. The lowest-order approximation (a "mean-field approximation to a mean-field approximation")

leads to a quadratic equation for $\epsilon(\omega)$ which is easily solved. For low frequencies ($\omega \to 0$), one finds

$$\sigma'(0)=\tfrac{1}{2}\sigma'_C(0;\bar{\phi})[3\lambda(\bar{\phi})-1] , \tag{5.1}$$

for $\lambda(\bar{\phi})>\frac{1}{3}$, and $\sigma'(0)=0$, for $\lambda(\bar{\phi})\leq\frac{1}{3}$. Thus a percolation transition with control parameter $\lambda(\bar{\phi})$ is predicted for strongly peaked local porosity distributions. Although the prediction of a percolation transition remains correct for arbitrary $\mu(\phi)$, the control parameter is in general not $\lambda(\bar{\phi})$. This will be seen in the next subsection. The percolation transition leads to a diverging dc dielectric constant, which is given within the present approximations as

$$\epsilon'(0)=\tfrac{1}{2}[3\lambda(\bar{\phi})-1]\epsilon'_C(0;\bar{\phi})+\frac{9\lambda(\bar{\phi})[\lambda(\bar{\phi})-1]\epsilon'_B(0;\bar{\phi})}{2[3\lambda(\bar{\phi})-1]} , \tag{5.2a}$$

for $\lambda(\bar{\phi})>\frac{1}{3}$, and as

$$\epsilon'(0)=\frac{\epsilon'_B(0;\bar{\phi})}{1-3\lambda(\bar{\phi})} , \tag{5.2b}$$

for $\lambda(\bar{\phi})<\frac{1}{3}$. Note that Eqs. (4.9) and (5.2) identify already two possible mechanisms for dielectric enhancement, one from the necessity of a thin-plate effect for *local* geometries in the high-porosity limit, the second from the percolation threshold.

In the high-frequency limit ($\omega \to \infty$), the results are

$$\epsilon'(\infty)=\frac{B}{4}\left[1\pm\left[1+\frac{8\epsilon'_C(\infty;\bar{\phi})\epsilon'_B(\infty;\bar{\phi})}{B^2}\right]^{1/2}\right] , \tag{5.3a}$$

where

$$B=[3\lambda(\bar{\phi})-1]\epsilon'_C(\infty;\bar{\phi})+\epsilon'_B(\infty;\bar{\phi})[2-3\lambda(\bar{\phi})] , \tag{5.3b}$$

for the real dielectric constant, and

$$\sigma'(\infty)=\frac{\lambda(\bar{\phi})\sigma'_C(\infty;\bar{\phi})\epsilon'(\infty)}{\lambda(\bar{\phi})\epsilon'_C(\infty;\bar{\phi})+[1-\lambda(\bar{\phi})]\epsilon'_B(\infty;\bar{\phi})\{[\epsilon'_C(\infty;\bar{\phi})+2\epsilon'(\infty)]/[\epsilon'_B(\infty;\bar{\phi})+2\epsilon'(\infty)]\}^2} , \tag{5.4}$$

for real part of the conductivity. The sign in Eq. (5.3a) has to be chosen such that σ' remains positive.

B. Low-frequency limit

In this subsection it will be shown that Eq. (3.2) does indeed imply the existence of a percolation threshold, also for general $\mu(\phi)$. But contrary to previous percolation theories for porous media, the bulk porosity $\bar{\phi}$ is not the control parameter of the transition. Therefore, a transition can or cannot occur as $\bar{\phi}$ is varied.

To identify the percolation transition, consider the low-frequency limit. Expanding Eq. (3.2) around $\omega=0$ leads to

$$\int_0^1 \frac{\sigma'_C(0;\phi)-\sigma'(0)}{\sigma'_C(0;\phi)+2\sigma'(0)}\lambda(\phi)\mu(\phi)d\phi + \int_0^1 \frac{\sigma'_B(0;\phi)-\sigma'(0)}{\sigma'_B(0;\phi)+2\sigma'(0)}[1-\lambda(\phi)]\mu(\phi)d\phi=0 , \tag{5.5}$$

for the effective dc conductivity $\sigma'(0)$ of the system. Inserting Eq. (4.6) into (5.5),

$$\sigma'(0)\int_0^1 \frac{\lambda(\phi)\mu(\phi)}{\sigma'_C(0;\phi)+2\sigma'(0)}d\phi = -\tfrac{1}{6}+\tfrac{1}{2}\int_0^1\lambda(\phi)\mu(\phi)d\phi \tag{5.6}$$

is found. This equation for $\sigma'(0)$ has no positive solutions if $\int_0^1\lambda(\phi)\mu(\phi)d\phi<\frac{1}{3}$. This identifies the control parameter for the transition as

$$p=\int_0^1\lambda(\phi)\mu(\phi)d\phi , \tag{5.7}$$

and the effective-medium value $p_c=\frac{1}{3}$ for the percolation threshold. The control parameter p is the total fraction of percolating local geometries.

For the effective real dielectric constant $\epsilon'(0)$, two equations are obtained. If $p<p_c$, the equation reads

$$[\epsilon'(0)]^{-1}\int_0^1 \frac{[1-\lambda(\phi)]\mu(\phi)}{[\epsilon'_B(0;\phi)]^{-1}+[2\epsilon'(0)]^{-1}}d\phi=2(p_c-p) . \tag{5.8}$$

For $p>p_c$ the solution to Eq.(5.6) must be inserted into

$$\epsilon'(0)=\frac{A+B}{C} , \tag{5.9}$$

where

$$A=[4\sigma'(0)]^{-1}\int_0^1\epsilon'_B(0;\phi)[1-\lambda(\phi)]\mu(\phi)d\phi ,$$

$$B=\int_0^1\frac{\epsilon'_C(0;\phi)\sigma'(0)}{[\sigma'_C(0;\phi)+2\sigma'(0)]^2}\lambda(\phi)\mu(\phi)d\phi ,$$

$$C=\int_0^1\frac{\sigma'_C(0;\phi)}{[\sigma'_C(0;\phi)+2\sigma'(0)]^2}\lambda(\phi)\mu(\phi)d\phi .$$

Equation (5.2) can be treated analogously to the case of ordinary percolation.[30,31] The effective conductivity $\sigma'(0)$ will be small for $p\to p_c$ or whenever $\bar{\phi}\to 0$, i.e., in the low-porosity limit. In this case the integral on the left-hand side of Eq. (5.6) is dominated by the small ϕ behavior of $\lambda(\phi)\mu(\phi)$. The following three cases for $\lambda(\phi)\mu(\phi)$ must be distinguished:

(a) $\int_0^1\phi^{-1}\lambda(\phi)\mu(\phi)d\phi<\infty$, (5.10a)

(b) $\lambda(\phi)\mu(\phi)\rightarrow$const for $\phi\rightarrow 0$, (5.10b)

(c) $\lambda(\phi)\mu(\phi)\propto\phi^{-\alpha}$ for $\phi\rightarrow 0$ and $0<\alpha<1$. (5.10c)

For case (a) the solution of Eq. (5.6) is obtained as

$$\sigma'(0)\approx\sigma'_{+}(p-p_c) , \tag{5.11}$$

where σ'_{+} is defined by

$$\frac{1}{\sigma'_{+}}=\int_0^1\frac{\lambda(\phi)\mu(\phi)}{\sigma'_C(0;\phi)}d\phi . \tag{5.12}$$

The integral exists because of Eq. (4.8) and condition (5.10a). Note that Eq. (5.11) is valid for all p for $\bar{\phi}\rightarrow 0$ and for all $\bar{\phi}$ for $p\rightarrow p_c$. The conductivity exponent $t=1$ has its expected reflective-medium value. The result of Eq. (5.11) is universal in the sense that the value of t does not depend on the specific geometry contained in $\lambda(\phi)$ and $\mu(\phi)$ as long as condition (5.10a) remains fulfilled.

The situation is very different for case (c). If $\lambda(\phi)\mu(\phi)\propto M\phi^{-\alpha}$ and $\sigma'_C(0;\phi)$ is given by Eq. (4.8), then to leading order in σ' the solution to Eq. (5.6) is

$$\sigma'(0)\propto C_1\left[\frac{1-\alpha}{M}\sin(\pi\alpha)(p-p_c)\right]^t , \tag{5.13a}$$

where the conductivity exponent

$$t=\frac{1}{1-\alpha} \tag{5.13b}$$

is now no longer universal. It depends on the behavior of $\lambda(\phi)\mu(\phi)$ for small ϕ. For the marginal case $\alpha=0$ [case (b)], logarithmic corrections to Eq. (5.11) are obtained, and

$$\sigma'(0)\propto(p-p_c)\left[\ln\left[\frac{1}{p-p_c}\right]\right]^{-1} . \tag{5.14}$$

For the real dielectric constant, Eq. (5.8) is valid below p_c. This equation has the same form as Eq. (5.6) for the conductivity. However, it is now the behavior of $\lambda(\phi)$ and $\mu(\phi)$ that high porosities $\phi\rightarrow 1$ that is relevant. From Eq. (5.8),

$$\epsilon'(0)\approx\epsilon'_{-}(p-p_c)^{-1} \tag{5.15}$$

is obtained, where

$$\epsilon'_{-}=\int_0^1\epsilon'_B(0;\phi)[1-\lambda(\phi)]\mu(\phi)d\phi , \tag{5.16}$$

analogous to Eqs. (5.11) and (5.12). Again, the expected value $s=1$ for the superconductivity exponent is universal as long as the integral in Eq. (5.16) exists. The asymptotic solution is valid for all p if $\bar{\phi}\rightarrow 1$, and for all $\bar{\phi}$ whenever $p\rightarrow p_c$. If $[1-\lambda(\phi)]\mu(\phi)\propto(1-\phi)^{-\beta}$, with $0<\beta<1$, then the superconductivity exponent becomes nonuniversal and has the value

$$s=\frac{1}{1-\beta} ,$$

in analogy with Eq. (5.13b) for the conductivity exponent t.

The central result of this section is the identification of a percolation transition underlying the random geometry of porous media. The control parameter for the transition is neither the bulk porosity $\bar{\phi}$ nor $\lambda(\bar{\phi})$ as suggested in Sec. V A, but the total fraction of conducting local geometries. Another result is that the underlying transition is expected to become relevant both in the low-porosity limit ($\bar{\phi}\rightarrow 0$) *and* in the high-porosity limit ($\bar{\phi}\rightarrow 1$). Having identified the transition using mean-field theory, the next step is to apply the results of scaling theory in the present context.

C. Scaling theory

In this section the scaling theory for the percolation transition[32,33] is applied in the present context.[34] Therefore, the present section goes beyond the effective-medium equation (3.2). Scaling theory starts from the assumption that the complex dielectric constant can be written as

$$\epsilon=\epsilon_{+}|p-p_c|^t f\left[\frac{\epsilon_{-}/\epsilon_{+}}{|p-p_c|^{t+s}}\right] , \tag{5.17}$$

with the scaling function

$$f(z)=A_0^{\mathrm{I}}+A_1^{\mathrm{I}}z+A_2^{\mathrm{I}}z^2+\cdots , \tag{5.18a}$$

for $|z|\ll 1$ and $p>p_c$,

$$f(z)=A_1^{\mathrm{II}}z+A_2^{\mathrm{II}}z^2+\cdots , \tag{5.18b}$$

for $|z|\ll 1$ and $p<p_c$, and

$$f(z)=A^{\mathrm{III}}z^{t/(t+s)}+\cdots , \tag{5.18c}$$

for $|z|\gg 1$ and all p. Here ϵ_{+} is the complex dielectric constant of a good conductor, and ϵ_{-} is the complex dielectric constant for the poor conductor. p is the volume fraction of good conductor, p_c is the percolation threshold, and t and s are the conductivity and the superconductivity exponents. For $\omega\rightarrow 0$, Eqs. (5.17) and (5.18) yield the well-known results

$$\sigma'(0)=A_0^{\mathrm{I}}\sigma'_{+}|p-p_c|^t+\cdots , \tag{5.19}$$

for $p>p_c$, and $\sigma'(0)=0$, for $p\leq p_c$ for the conductivity. For the dielectric constant, one obtains

$$\epsilon'(0)=A_1^{\mathrm{II}}\epsilon'_{-}|p-p_c|^{-s}+\cdots , \tag{5.20a}$$

for $p<p_c$, and

$$\epsilon'(0)=A_0^{\mathrm{I}}\epsilon'_{+}|p-p_c|^t+A_1^{\mathrm{I}}\epsilon'_{-}|p-p_c|^{-s}+\cdots , \tag{5.20b}$$

for $p>p_c$.

For one-dimensional systems, the effective-medium approximation is known to be asymptotically exact for class (a) distributions.[31] If this remains true in higher dimensions, then the scaling theory can be applied to porous media by identifying the prefactors σ'_{+} and ϵ'_{-} above as those given in Eqs. (5.12) and (5.16). The important new aspect of Eqs. (5.19) and (5.20) applied to porous media is that they are universally valid in the low-porosity limit of systems having $\lambda(\phi)\mu(\phi)$ which obeys condition (5.10a). Naturally, they are also valid whenever $p\rightarrow p_c$ at finite $\bar{\phi}$.

Consider now the case of finite frequencies $\omega\neq 0$. The condition $|z|\ll 1$ in Eqs. (5.18) is always satisfied for

sufficiently small ω. On the other hand, the condition $|z| \gg 1$ is always satisfied if either $p \approx p_c$ or $\epsilon'_-/\epsilon'_+ \gg 1$. The latter condition does not apply for the systems considered in this paper, and thus $|z| \gg 1$ is always interpreted as $p \approx p_c$. Equations (5.17) and (5.18) imply, for the case $p < p_c$,

$$\sigma'(\omega) = -A_2^{\mathrm{II}} \sigma'_+ |p - p_c|^{-2s-t} \omega^2 + \cdots , \tag{5.21}$$

for the conductivity, and

$$\epsilon'(\omega) = A_1^{\mathrm{II}} \epsilon'_- |p - p_c|^{-s} + A_2^{\mathrm{II}} \epsilon'_- |p - p_c|^{-2s-t} \left[\frac{\epsilon'_-}{\epsilon'_+} \right] \left[\frac{\omega}{\omega_+} \right]^2 + \cdots , \tag{5.22}$$

for the dielectric constant, where $\omega_+ = \sigma'_+/\epsilon'_+$. For $p \approx p_c$ one obtains

$$\sigma'(\omega) = A^{\mathrm{III}} \sigma'_+ \left[\frac{\epsilon'_-}{\epsilon'_+} \right]^{t/(t+s)} \left[\frac{\omega}{\omega_+} \right]^{t/(t+s)} \times \left[\cos \left[\frac{\varphi t}{t+s} \right] + \frac{\omega}{\omega_+} \sin \left[\frac{\varphi t}{t+s} \right] \right] + \cdots \tag{5.23}$$

and

$$\epsilon'(\omega) = A^{\mathrm{III}} \epsilon'_+ \left[\frac{\epsilon'_-}{\epsilon'_+} \right]^{t/(t+s)} \left[\frac{\omega_+}{\omega} \right]^{s/(t+s)} \times \left[\sin \left[\frac{-\varphi t}{t+s} \right] + \frac{\omega}{\omega_+} \cos \left[\frac{\varphi t}{t+s} \right] \right] + \cdots , \tag{5.24}$$

where $\varphi = \arg(\epsilon_-/\epsilon_+)$. Finally, the case $p > p_c$ leads to

$$\sigma'(\omega) = \sigma'_+ (A_0^{\mathrm{I}} |p - p_c|^t - A_2^{\mathrm{I}} |p - p_c|^{-2s-t} \omega^2 + \cdots) \tag{5.25}$$

and

$$\epsilon'(\omega) = A_0^{\mathrm{I}} \epsilon'_+ |p - p_c|^t + A_1^{\mathrm{I}} \epsilon'_- |p - p_c|^{-s} + A_2^{\mathrm{I}} \epsilon'_- |p - p_c|^{-2s-t} \left[\frac{\epsilon'_-}{\epsilon'_+} \right] \left[\frac{\omega}{\omega_+} \right]^2 + \cdots . \tag{5.26}$$

These results predict a divergence of $\epsilon'(\omega)$ as $\omega \to 0$ with an exponent $s/(s+t)$ whenever the control parameter p approaches criticality. Simultaneously, the conductivity will also exhibit power-law behavior with exponent $t/(t+s)$. Outside the critical region, the frequency dependence is quadratic.

D. Archie's law

Most publications on the electrical properties of porous media discuss the phenomenological relationship[8] between dc conductivity and bulk porosity:

$$\sigma'(0) \propto \bar{\phi}^m \tag{5.27}$$

called "Archie's law," which is usually written in terms of the formation factor $F = [\sigma'(0)]^{-1}$. The widespread acceptance of Eq. (5.27) as a fundamental law for the physics of porous media is rather surprising in view of the fact that most experimental data[1,2,3,6,17] rarely span more than a decade in porosity. Correspondingly, the cementation exponent m is found to scatter widely between $m \approx 1$ and $m \approx 4$. Having found it necessary to introduce two functions to only partially characterize the pore-space geometry, it may be understandable that the present author has strong reservations to accept $\bar{\phi}$ and m as sufficient geometric information to predict σ', as is done in the well-logging literature.[1] However, he feels compelled to admit that Eq. (5.27) receives a certain amount of theoretical justification from his own investigation, if it is interpreted not as a relation between geometry and electrical resistance, but as a statement about physical processes which reduce the bulk porosity. Let me explain this in more detail.

Sedimentary and related rocks arise from sedimentation and subsequent compactification, cementation, and other physicochemical processes. The bulk porosity $\bar{\phi}$ changes during the sedimentation history of the rock. The final specimen's porosity may be primary, i.e., interparticle porosity, or secondary, i.e., resulting from dissolution of grains or cements, shrinkage, fracturing, etc. The diagenetic processes change the local dielectric and geometric properties. Within the present formulation, it might be assumed that primarily $\lambda(\phi)$ and $\mu(\phi)$ are affected. This implies that σ'_+ and p become implicitly dependent upon $\bar{\phi}$, and consequently $\sigma'(0)$ will change with $\bar{\phi}$. To discuss these changes one needs a physical model for the changes of λ and μ, but this is not the objective of the present investigation. Nevertheless, it is of interest to discuss the general consequences of the scaling approach presented above. Clearly, $\sigma'_+(\bar{\phi})$ should tend to zero as $\bar{\phi} \to 0$, and it should approach σ'_W for $\bar{\phi} \to 1$. It seems also plausible that $p(\bar{\phi})$ should decrease as $\bar{\phi}$ is lowered. If one assumes that $\sigma'_+(\bar{\phi})$ and $p(\bar{\phi})$ can be expanded around $\bar{\phi} = 0$ as

$$\sigma'_+(\bar{\phi}) = \dot{\sigma}'_+(0)\bar{\phi} + \tfrac{1}{2}\ddot{\sigma}'_+(0)\bar{\phi}^2 + \cdots , \tag{5.28}$$

$$p(\bar{\phi}) = p(0) + \dot{p}(0)\bar{\phi} + \cdots , \tag{5.29}$$

then Eq. (5.19) implies that

$$\sigma'(\bar{\phi}) = A_0^{\mathrm{I}} \dot{\sigma}'_+(0) \bar{\phi} [p(0) - p_c + \dot{p}(0)\bar{\phi} + \cdots]^t . \tag{5.30}$$

This already resembles Eq. (5.27). In particular, if it happens that $p(0) \approx p_c$, i.e., if one approaches criticality as $\bar{\phi} \to 0$, then Eq. (5.30) yields Archie's law with a cementation exponent,

$$m = 1 + t , \tag{5.31a}$$

as long as condition (5.10a) remains satisfied during the cementation process. if the system falls under condition (5.11c), however, the cementation index becomes

$$m = 1 + t + \frac{\alpha(\bar{\phi})}{1 - \alpha(\bar{\phi})} . \tag{5.31b}$$

Note that α and thus m may explicitly depend on the bulk porosity. Even more complicated results for m are obtained if $\lambda(\phi)$ and $\mu(\phi)$ change with $\bar{\phi}$ such that $\sigma'_+(\bar{\phi}) \propto \bar{\phi}^{m_\sigma}$ and $p(\bar{\phi}) \propto p_c + \dot{p}(0)\bar{\phi}^{m_p}$. In such cases,

$$m = m_\sigma + m_p \left[t + \frac{\alpha(\bar{\phi})}{1-\alpha(\bar{\phi})} \right] . \tag{5.31c}$$

The surprising result is that the simplest form for m, namely, Eq. (5.31a), predicts an exponent in the range from $m=2$ for $p \gg p_c$ to $m = 1+t \approx 3$ for $p \approx p_c$. Nevertheless, the cementation exponent will in general be very different for different compaction processes, and without physical models for such processes even a nonmonotonous behavior of $\sigma'(0;\bar{\phi})$ is possible. The important result of this section is that it provides a general framework inside which the apparent phenomenological universality and scaling properties of Archie's law might be understood.

A second interesting consequence of this section is that it predicts similar scaling laws for the dielectric constant in the *high-porosity limit* $\bar{\phi} \to 1$. This is a consequence of the thin-plate effect [Eq. (4.9)] and analogous assumptions about the corresponding dilution process. More precisely, it is predicted that

$$\epsilon'(0) \propto (1-\bar{\phi})^{-m'} . \tag{5.32}$$

Here the "dilution exponent" m' is given in the simplest case as

$$m' = 1 + s , \tag{5.33a}$$

where s is the superconductivity exponent, and in the general case as

$$m' = m'_\sigma + m'_p \left[s + \frac{\beta(\bar{\phi})}{1-\beta(\bar{\phi})} \right] . \tag{5.33b}$$

The exponents m'_σ and m'_p characterize the behavior of ϵ'_- and p as $\bar{\phi} \to 1$, and $\beta(\bar{\phi})$ is the exponent governing $\lambda(\phi)\mu(\phi)$ as $\bar{\phi} \to 1$. The behavior predicted by Eq. (5.32) might be experimentally observable in water-filled pore casts of systems obeying (5.27).

VI. MODEL CALCULATIONS

This section returns to Eq. (3.2) and presents numerical solutions. This is intended as a case study exploring the relationship between the statistics of local geometries and bulk dielectric behavior. The main focus will be on dielectric enhancement. To solve Eq. (3.2) for $\epsilon(\omega)$, one must know the geometric input functions $\mu(\phi), \lambda(\phi)$ and the local dielectric responses $\epsilon_C(\omega;\phi), \epsilon_B(\omega;\phi)$. Unfortunately, no experimental data are available at present,[27] and geometric modeling has to be used instead.

A. Local dielectric response

The hypothesis of local simplicity states that the local geometries are simple and that the effective local dielectric constants are insensitive to geometrical details other than local porosity. The simplest isotropic local geometry is spherical. For conducting local geometries, a water-coated spherical rock grain will serve as the local model. For blocking geometries a rock-coated spherical water pore is employed. In the notation of Sec. IV, this means

$$\epsilon_C(u;\phi) = \epsilon_W \left[1 - \frac{1-\phi}{(1-\epsilon_R/\epsilon_W)^{-1} - \frac{1}{3}\phi} \right] , \tag{6.1}$$

$$\epsilon_B(u;\phi) = \epsilon_R \left[1 - \frac{\phi}{\left[1 - \frac{\epsilon_W}{\epsilon_R} \right]^{-1} - \frac{1}{3}(1-\phi)} \right] . \tag{6.2}$$

In the low-frequency limit, one obtains for the conducting geometry

$$\sigma'_C(0;\phi) = \sigma'_W \frac{2\phi}{3-\phi} = \tfrac{2}{3}\sigma'_W \phi (1 + \tfrac{1}{3}\phi + \cdots) , \tag{6.3}$$

thereby identifying C_1 in Eq. (4.8) as $C_1 = \frac{2}{3}\sigma'_W$. The real dielectric constant is found as

$$\epsilon'_C(0;\phi) = \epsilon'_W - \frac{1-\phi}{(1-\frac{1}{3}\phi)^2} [\epsilon'_W (1 - \tfrac{1}{3}\phi) - \epsilon'_R] . \tag{6.4}$$

For the blocking geometry, the dc limit gives $\sigma'_B(0;\phi) = 0$, in agreement with Eq. (4.6), and

$$\epsilon'_B(0;\phi) = \epsilon'_R \frac{1+2\phi}{1-\phi} , \tag{6.5}$$

for $\phi < 1$, identifying $B_1 = 1/\epsilon'_R$ in Eq. (4.9), and $\epsilon'_B(0;\phi) = \epsilon'_W$, for $\phi = 1$. Note the presence of the thin-plate divergence in the $\phi \to 1$ limit.

B. Local porosity distribution

It was mentioned repeatedly that no experimental data for $\mu(\phi)$ are available to the author at present. A qualitative guideline for porous media resulting from spinodal decomposition might be the shape of the order-parameter distribution calculated in Ref. 28, which suggests in particular that $\mu(\phi)$ can be bimodal.

For the subsequent calculations, a simple mixture of two β distributions has been used. The analytic expression reads

$$\mu(\phi) = w \frac{\Gamma(\mu_1+\nu_1)}{\Gamma(\mu_1)\Gamma(\nu_1)} (1-\phi)^{\mu_1 - 1} \phi^{\nu_1 - 1} + (1-w) \frac{\Gamma(\mu_2+\nu_2)}{\Gamma(\mu_2)\Gamma(\nu_2)} (1-\phi)^{\mu_2 - 1} \phi^{\nu_2 - 1} , \tag{6.6}$$

where $0 \le w \le 1$, $\mu > 0$, $\nu > 0$, and $\Gamma(x)$ denotes Euler's Γ function. The bulk porosity is then given as

$$\bar{\phi} = w \frac{\nu_1}{\mu_1+\nu_1} + (1-w) \frac{\nu_2}{\mu_2+\nu_2} . \tag{6.7}$$

For $\mu, \nu > 1$, the β densities are bell shaped, and for $\mu, \nu < 1$ they diverge at the limits.

Eight different local porosity distributions are compared in the calculations. All of them are chosen such that they give the same bulk porosity $\bar{\phi} = 0.1$. The values of the parameters are listed in Table I, and the densities

TABLE I. Parameter values for the eight different forms of $\mu(\phi)$ displayed in Fig. 1 and used in the model calculations. The parameters w, μ_1, ν_1, μ_2, and ν_2 are those of Eq. (6.6). $\bar{\phi}_1$, $\bar{\phi}_2$, var_1, and var_2 are the average and variance for μ_1,μ_2 if μ in Eq. (6.6) is written as $\mu=w\mu_1+(1-w)\mu_2$. The rows labeled $\bar{\phi}$, variance, and skewness contain the mean, variance, and skewness for the eight forms of $\mu(\phi)$.

Curve No.	1	2	3	4	5	6	7	8
w	1	1	2/3	1	1	1	2/3	2/3
μ_1	1.0	360.0	191.1	7.2	4.5	1.8	28.8	58.6
ν_1	1.000	40.000	3.900	0.800	0.500	0.200	0.087	0.176
μ_2			1423.0				13.9	2.24
ν_2			500.00				6.00	0.96
$\bar{\phi}_1$	0.1	0.1	0.02	0.1	0.1	0.1	0.003	0.003
$\bar{\phi}_2$			0.26				0.294	0.294
var_1	0.003 33	0.000 24	0.000 10	0.000 10	0.015 00	0.030 00	0.000 10	0.000 05
var_2			0.000 10				0.010 00	0.050 00
$\bar{\phi}$	0.1	0.1	0.1	0.1	0.1	0.1	0.1	0.1
Variance	0.003 33	0.000 24	0.012 90	0.010 00	0.015 00	0.030 00	0.022 13	0.035 41
Skewness	0	0.2657	0.6993	1.6004	1.8679	2.3124	1.1588	2.1176

themselves are displayed graphically in Fig. 1. Each distribution is identified by a number and a line style as indicated in the inset of Fig. 1. $\bar{\phi}_i$ $(i=1,2)$ are the partial porosities $\nu_i/(\nu_i+\mu_i)$ in Eq. (6.7). The uniform distribution carries number 1 and is identified by a thin dot-dashed line. Number 2 represents the strongly peaked case and is identified by a wide dashed thin line, and so on.

The choices presented in Fig. 1 are arbitrary. The reader should bear in mind, however, that $\mu(\phi)$ is easily measurable and *cannot* be adjusted to fit experimentally observed dielectric data when comparing the theory with experiment. The choices for $\mu(\phi)$ presented here are intended as a case study illustrating different possibilities

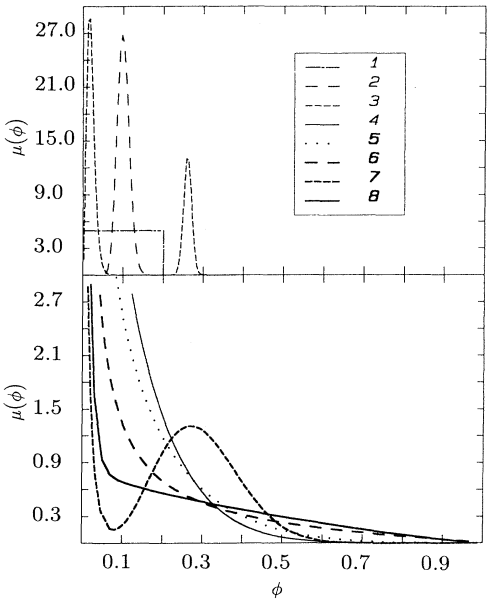

FIG. 1. Eight local porosity densities with parameters given in Table I.

that might occur in real or artificial experimental systems. The highly peaked $\mu(\phi)$ (curve 2) represents the limit of weak disorder. Remember that $\mu(\phi)=\delta(\phi-\bar{\phi})$ for ordered systems. Curve 2 gives a reference to which other distributions can be compared. The distributions 4, 5, and 6 have been chosen divergent at $\phi=0$ with exponents 0.8, 0.5, and 0.2 as examples for distributions whose inverse first moment does not exist. Curves 3, 7, and 8 demonstrate the fact that $\mu(\phi)$ itself might be "of percolation type." This occurs if the porous medium contains two types of porosity or regions of very different porosities. For curve 3 the ratio between the two porosities is roughly 100, and the inverse first moment of $\mu(\phi)$ exists. For curves 7 and 8, the ratio is roughly 1000, and the densities diverge at $\phi=0$. In all cases the distributions were chosen critical in the sense that the weight for the higher-porosity component is $\frac{1}{3}$.

C. Local percolation probability

The local percolation probabilities $\lambda(\phi)$ can be measured simultaneously with the local porosity distribution $\mu(\phi)$. However, such a measurement is more difficult because it requires the approximate reconstruction of the three-dimensional pore space from parallel two-dimensional sections. For this reason geometric modeling of porous media is most important for this quantity.

Three simple models will be compared in the calculations: the uniformly connected model (UCM), the central pore model (CPM), and the grain consolidation model (GCM).

1. Uniformly connected models

In these models $\lambda(\phi)$ equals a constant, i.e.,

$$\lambda(\phi)=p \ . \tag{6.8}$$

In the simplest case, the fully connected model, $p=1$. This means that all local geometries are assumed to be

conducting. In addition, the case $p=\frac{1}{2}$ will also be investigated.

2. Central pore model

Consider a cubic cell of volume 1 filled with rock. Inside the cubic cell a centered cubic pore of side length a $(0\leq a\leq 1)$ is cut out. Now a random process is used to drill cylindrical pores with square cross section from the faces of the cube toward the central pore. Sometimes these pores will connect to the central pore, and sometimes not. The random process starts with the choice of an arbitrary face of the cube. Now choose a random number r between 0 and $\frac{1}{2}$. If $r>\frac{1}{2}(1-a)$, a pore with square cross section of side length b $(0\leq b\leq a)$ is drilled from the center of the face all the way to the central pore. The central pore had volume a^3, and the connection pore has the volume $\frac{1}{2}b^2(1-a)$. If the random number fulfills $f<\frac{1}{2}(1-a)$, then the face is not pierced, but instead the same volume $\frac{1}{2}b^2(1-a)$ is removed from the wall in such a way that the resulting pore space remains disconnected from the pore space connected to the central pore. This process is repeated for all six faces of the cube. The cubic symmetry is not essential, and a model with different symmetry can be defined similarly.

The result of the process described above is a cubic cell whose porosity can be expressed in terms of the side length a of the central pore and the ratio $R=b/a$ as

$$\phi=a^3+3b^2(1-a)=a^3(1-3R^2)+3R^2a^2 . \tag{6.9}$$

According to the definitions in Sec. II, the cell is called percolating if there exist at least one path within the pore space connecting a face to a face different than itself. To obtain $\lambda(\phi)$ the probability that either no or exactly one face is pierced has to be calculated. This probability equals $1-\lambda(\phi)$. Clearly,

$$1-\lambda=(1-a)^6+a(1-a)^5=(1-a)^5 . \tag{6.10}$$

Thus, in the central pore model,

$$\lambda(\phi,R)=1-[1-a(\phi,R)]^5 , \tag{6.11}$$

where $a(\phi,R)$ is that root of Eq. (6.9), which fulfills $0\leq a\leq 1$ for all $0\leq\phi\leq 1$ and $0\leq R\leq 1$. For $R=1$, i.e., $b=a$, it follows that $\phi\propto a^2$ and thus $a\propto\phi^{1/2}$, resulting in $\lambda(\phi)\propto\phi^{1/2}$ for small ϕ. On the other hand, for $R\to 0$ one finds $a\propto\phi^{1/3}$ for $\phi\to 0$ and thus $\lambda(\phi)\propto\phi^{1/3}$ for $\phi\to 0$. Thus the general conclusion for the central pore model is that

$$\lambda(\phi)\propto\phi^{\gamma} , \tag{6.12}$$

where γ can range between $\frac{1}{2}$ and $\frac{1}{3}$.

3. Grain consolidation model

The grain consolidation model was proposed as a simple geometrical model for diagenesis.[11] Its main observation is the existence and smallness of the percolation threshold in regular and random bead packings when the bead radii are increased. In fact, the model has recently been modified such that the critical porosity at which conduction ceases can be arbitrarily small.[12] For regular bead packings, this implies

$$\lambda(\phi)=\begin{cases}0 & \text{for } \phi<\phi_c\\ 1 & \text{for } \phi>\phi_c\end{cases} . \tag{6.13}$$

For random packings $\lambda(\phi)$ will be smoothed out around ϕ_c. For simplicity, in this paper Eq. (6.13) will be used with $\phi_c=0.05$.

The most important aspect of $\lambda(\phi)$ is that it determines the control parameter p. According to Eq. (6.12), its behavior near $\phi=0$ can influence the exponent α in (5.10c). Note that for the grain consolidation model the form of $\lambda(\phi)$ always implies that condition (5.10a) is fulfilled, and universal behavior is expected. The half-connected model in the uniformly connected model class is included to demonstrate the influence of the thin-plate effect. The shape of $\lambda(\phi)$ in all other cases gives extremely small probability to blocking geometries with high porosities. This is expected to be generally true for interparticle porosity. However, the secondary pore space in real rocks may contain a significant fraction of high-porosity blocking geometries.[32]

D. Numerical results

Numerical solutions to Eq. (3.2) were obtained using an iterative technique. The iteration was stopped whenever $|\epsilon_n(\omega)-\epsilon_{n-1}(\omega)|<10^{-7}$. In Figs. 2–5 selected results for $\epsilon(\omega)$ are presented. Figure 2 presents the uniformly connected model with $p=1$, Fig. 3 the uniformly connected model with $p=\frac{1}{2}$. Figure 4 gives the results for the central pore model with $R=0.922$, and Fig. 5 those for the grain consolidation model with $\phi_c=0.05$. In each figure the line styles correspond to the line styles of the local porosity distributions displayed in Fig. 1. Part (a) of each figure shows $\log_{10}\epsilon'(\omega)$ as a function of $\log_{10}\omega$ in the upper graph and $\log_{10}\sigma'(\omega)$ in the lower graph. In addition, the inset in the upper right-hand corner displays the local percolation probability $\lambda(\phi)$ for $0\leq\phi\leq\frac{1}{2}$. The vertical scale for the inset is always $0\leq\lambda\leq 2$. Part (b) displays in the upper graph $-d[\log_{10}\epsilon'(\omega)]/d(\log_{10}\omega)$ versus $\log_{10}\omega$ and $d[\log_{10}\sigma'(\omega)]/d(\log_{10}\omega)$ in the lower plot. These quantities give a more sensitive representation of the dispersion and show at the same time the values of "local exponents." In all figures frequency is measured in units of the relaxation frequency of water as discussed in Sec. IV. All plots are given over ten frequency decades with a resolution of five points per decade.

The absolute dispersion for all figures is collected in Table II. $\Delta\epsilon$ is defined as $\Delta\epsilon=\epsilon'(0)-\epsilon'(\infty)$, while $\Delta\sigma=\sigma'(\infty)-\sigma'(0)$.

E. Discussion

It is obvious from Figs. 2–5 [especially part (b)] that the low-frequency dielectric response depends sensitively on the details of $\mu(\phi)$ and $\lambda(\phi)$. A general discussion is difficult, because the response is always a mixture between three basic mechanisms each of which can give

significant dielectric dispersion. The first mechanism is the dispersion resulting from the disorder in $\mu(\phi)$ itself. The second mechanism is the dispersion resulting from p, i.e., from percolation geometry. The third mechanism is the dispersion resulting from the behavior of $\lambda(\phi)$ in the $\phi \rightarrow 1$ limit, i.e., the thin-plate effect.

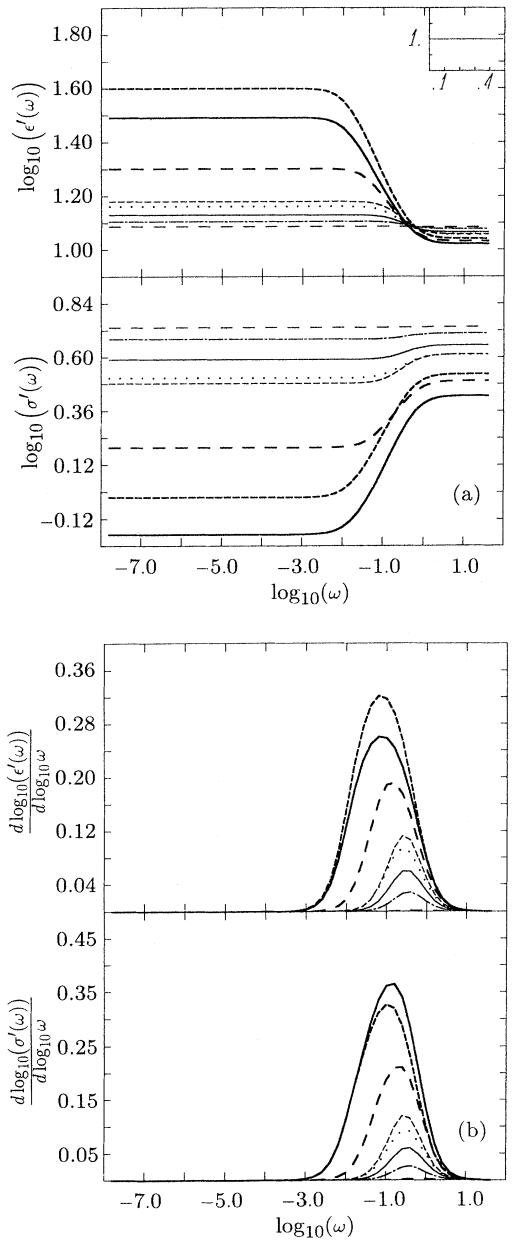

FIG. 2. (a) Real part of the complex dielectric constant (upper graph) and real part of complex conductivity (lower graph) vs frequency in a doubly logarithmic plot. Each graph contains eight curves whose line style corresponds to the local porosity densities displayed in Fig. 1. The inset shows the local percolation probability $\lambda(\phi)$ used in the calculation, in this case that of the uniformly conducting model with $p=1$. The vertical axis of the inset ranges from $\lambda=0$ to 2, the horizontal axis from $\phi=0$ to 0.5. (b) Derivatives of the curves in (a).

Before discussing the three mechanisms, it is important to note that the bulk porosity $\bar{\phi}$ does not influence the shape of the response curves if it is changed without changing the shape of $\mu(\phi)$. Instead, it determines an overall frequency shift for the frequency region over which the dispersion occurs. As $\bar{\phi}$ is lowered, this region is shifted toward lower frequencies. This observation together with the fact that all $\mu(\phi)$ give the same bulk porosity of 0.1 shows that the bulk porosity by itself cannot be used to characterize the dielectric response. In particular, there is no theoretical basis for Archie's law [Eq. (5.27)] if interpreted as a relation between dc con-

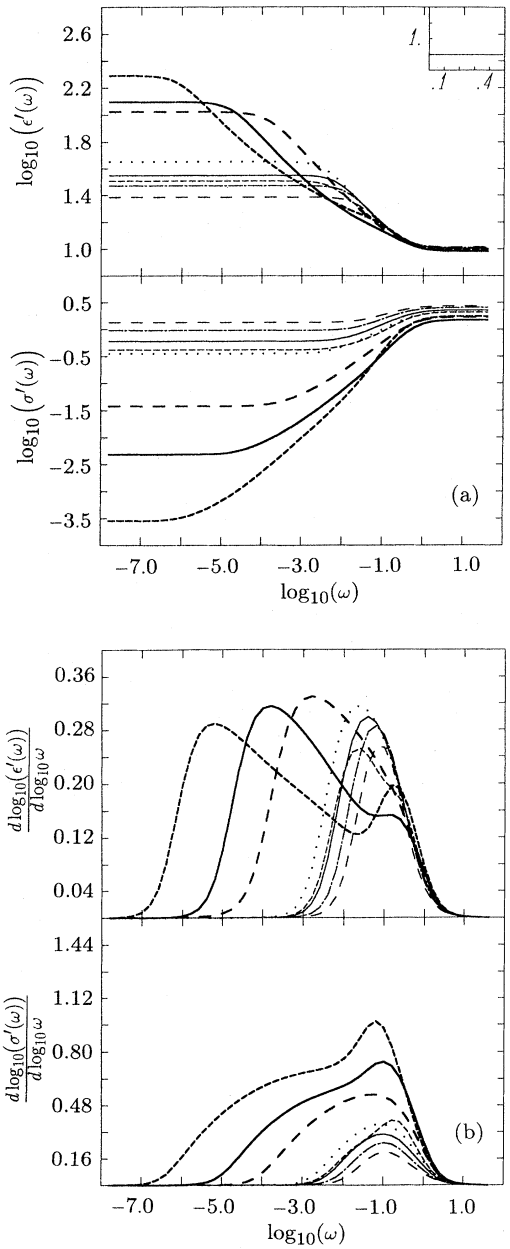

FIG. 3. Same as Fig. 2 for the uniformly conducting model with $p=\frac{1}{2}$.

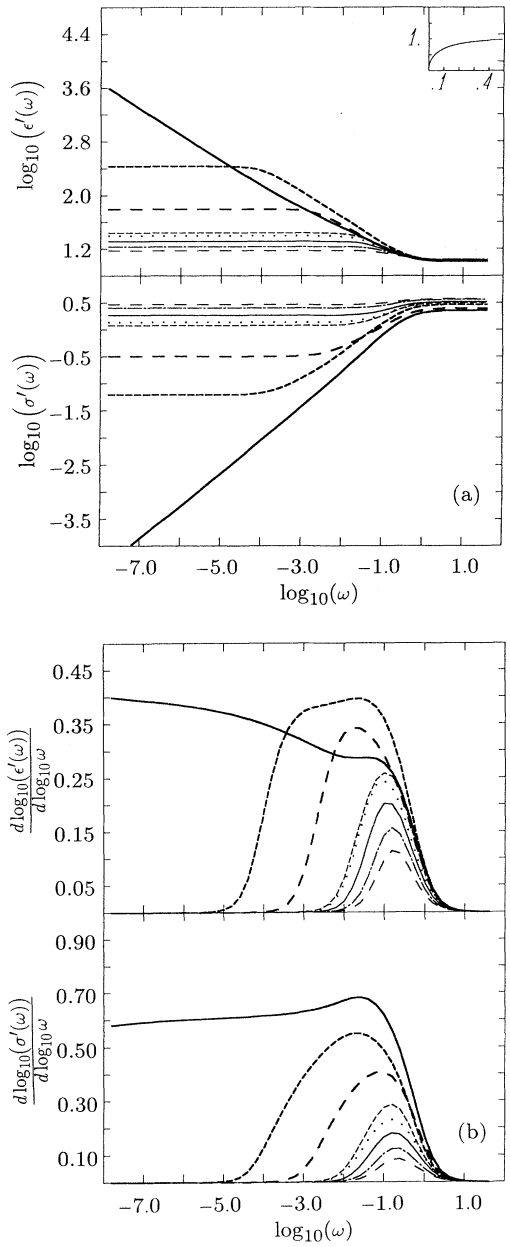

FIG. 4. Same as Fig. 2 for the central pore model with $R=0.922$.

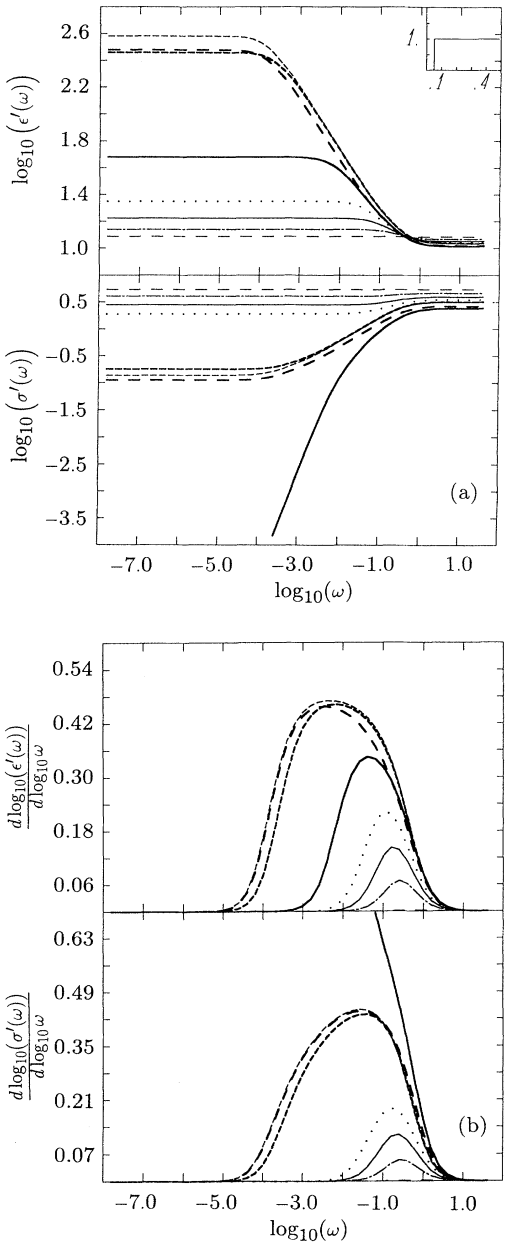

FIG. 5. Same as Fig. 2 for the grain consolidation model with $\phi_c=0.05$.

TABLE II. Numerical values for $\Delta\epsilon=\epsilon'(0)-\epsilon'(\infty)$ and $\Delta\sigma=\sigma'(\infty)-\sigma'(0)$ obtained in the model calculations of Figs. 2–5.

Curve No.	1	2	3	4	5	6	7	8
$\Delta\epsilon$ (Fig. 2)	0.798	0.053	3.716	1.863	3.147	9.261	28.793	20.484
$\Delta\sigma$ (Fig. 2)	0.298	0.035	1.067	0.619	0.889	1.545	2.400	2.029
$\Delta\epsilon$ (Fig. 3)	19.197	13.819	21.956	25.162	34.950	96.046	186.010	115.270
$\Delta\sigma$ (Fig. 3)	1.585	1.370	1.664	1.674	1.741	1.648	1.751	1.489
$\Delta\epsilon$ (Fig. 4)	5.996	3.835	16.616	9.639	14.204	52.196	259.700	3932.522
$\Delta\sigma$ (Fig. 4)	1.105	0.801	1.974	1.455	1.708	2.176	2.877	2.283
$\Delta\epsilon$ (Fig. 5)	2.119	0.053	371.525	5.498	11.430	291.481	277.396	37.691
$\Delta\sigma$ (Fig. 5)	0.595	0.035	3.025	1.137	1.604	2.565	3.043	2.436

ductivity and bulk porosity (see Sec. V D for a discussion).

A second observation is that in all figures the high-frequency real dielectric constant $\epsilon'(\infty)$ is not very sensitive to the details of $\mu(\phi)$. This is a consequence of the fact that for low $\bar{\phi}$ the local dielectric constants ϵ'_B and ϵ'_C must both approach ϵ'_R.

The first mechanism, dispersion from the form of $\mu(\phi)$, can be studied in pure form when $\lambda(\phi)=1$, and the corresponding results are shown in Fig. 2. In this case there are no blocking local geometries; i.e., $p=1$ according to Eq. (5.7). If $\mu(\phi)$ is highly peaked as in curve 2, then the system is only weakly disordered, and there is almost no visible dispersion in the dielectric response. The dispersion increases with the amount of disorder contained in $\mu(\phi)$. In fact, distributions with power-law divergences at $\phi\rightarrow 0$ or with percolation structure generate the strongest dispersion, as can be seen from curves 3 and 5–8 in Fig. 2. Table II shows that the dispersion varies almost three orders of magnitude between the different distributions. Note that relatively similar local porosity distributions such as curves 6 and 8 can have very different dielectric response. On the other hand, very different shapes for $\mu(\phi)$ can give similar $\epsilon(\omega)$, as demonstrated by curves 3 and 5. This shows that the dielectric response by itself does not contain a full geometric characterization of the pore space, and it needs always to be complemented with additional physical or geometrical information. This is not too surprising. Indeed, it is more surprising that when the dielectric response becomes large it is also very sensitive to geometric details. This is the case for dielectric enhancement near the percolation threshold or as a result of the thin-plate effect.

Consider the thin-plate mechanism. It requires the presence of blocking geometries of high porosity. Mathematically, this means $\lambda(\phi)\neq 1$ for large ϕ. As a simple illustration, Fig. 3 displays the results for the uniformly connected model when $\lambda(\phi)=\frac{1}{2}$. Now $p=\frac{1}{2}$, which is far away from p_c. Nevertheless, the dielectric dispersion is much stronger than would be obtained for solutions to the central pore model or grain consolidation model with the same p. Compare, e.g., curve 5 in Fig. 3 with curve 5 in Fig. 5. Moreover, the dielectric dispersion becomes sensitive to the details $\mu(\phi)$. It is now possible to distinguish in Fig. 3(b) the distributions 3, 7, and 8, which have $w\neq 1$ from the rest for which $w=1$. In particular, curves 3 and 5, which had very similar response in Fig. 2, appear now very different. The dispersion is the stronger the more weight $\mu(\phi)$ has at high ϕ. This can be seen from curve 3, which shows less dispersion than curves 4 and 5, while the opposite was true for Fig. 2. Similarly, ϵ' for curve 7 is depressed below curves 6 and 8 at intermediate frequencies. At very low frequencies, the percolative character of distribution 7 is responsible for stronger overall dispersion than in curve 6. The degree of asymmetry of $\mu(\phi)$ is reflected in the asymmetry of the response, as best seen in the derivatives plotted in Fig. 3(b).

The percolation mechanism is responsible for strong dielectric dispersion in Figs. 4 and 5. There is essentially no dispersion from the thin-plate mechanism in these cases because in both cases $\lambda(\phi)\approx 1$ for $\phi>0.5$, and thus there are no local geometries with a high dielectric constant. Figure 4 represents the central pore model with $R=0.922$, and results for the grain consolidation model with $\phi_c=0.05$ are given in Fig. 5. Contrary to the situation in Figs. 2 and 3, p is now different for each distribution. The results of performing the integral in Eq. (5.7) are listed in Table III. Naturally, the dielectric dispersion increases strongly with $p\rightarrow p_c$ and this effect dominates the dispersion from μ itself. In particular, for $p\approx p_c$ power-law behavior for $\epsilon(\omega)$ as a function of frequency is obtained in agreement with the scaling theory presented in Sec. V. As an example, scaling theory predicts the exponent 0.597 for the conductivity of distribution 8 in Fig. 4 and 0.403 for the real dielectric constants. These predictions are obtained from Eqs. (5.23) and (5.24) using $s=1$ and Eqs. (5.13b) and (6.12) with $\gamma=0.5$, and the exponent ν_1 from Table I. Figure 4(b) shows that these values are indeed approached at low frequencies. Similarly, scaling theory predicts the exponent 0.5 for ϵ' and σ' corresponding to distributions 3, 6, and 7 in Fig. 5. Again, these values are approached as seen from Fig. 5(b), although the power-law behavior occurs over a limited frequency range because p is not sufficiently close to the critical region. Note that curve 8 in Fig. 5 has dropped below the percolation threshold, and thus the conductivity increases as ω^2 for small ω.

The complexity and variability of $\epsilon(\omega)$ obtained from the simple mean-field solutions of this section correspond to the complexity and variability of possible pore-space geometries. More approximate analytical investigations of the solutions to Eq. (3.2) are necessary to identify simple parameters characterizing μ and λ which allow a better classification of the solutions and thereby the possible geometries.

F. Sedimentary rock

The present paper deals only with simple homogeneous and isotropic porous media. Real rocks are highly inhomogeneous, but they can also be discussed within the

TABLE III. Calculated values of p corresponding to the eight different forms of $\mu(\phi)$ for the central pore model (CPM, displayed in Fig. 4) and for the grain consolidation model (GCM, displayed in Fig. 5). Note that $p=1$ for all cases in Fig. 1, and $p=\frac{1}{2}$ for all cases displayed in Fig. 2.

Curve No.	1	2	3	4	5	6	7	8
CPM	0.6542	0.6940	0.5420	0.5858	0.5341	0.4059	0.3643	0.3334
GCM	0.7500	1.0000	0.3399	0.6048	0.4962	0.3415	0.3376	0.2841

present framework. Sedimentary rocks exhibit two main types of porosity. Primary interparticle porosity is the porosity between the grains of the original sediment. Often, this pore space is changed during diagenesis of the sediment. In particular cements between the grains can exhibit a qualitatively different secondary porosity.[33] This situation can be treated within the present formalism by replacing the dielectric constant ϵ_W of the pore-filling fluid with the effective dielectric constant of the pore-filling cement. Naturally, the results must be much more complex, as they contain additional independent geometrical information describing the cement.

VII. INVERSE PROBLEM

Up to now the direct problem was discussed which consists in finding $\epsilon(\omega)$ for given $\mu(\phi)$ and $\lambda(\phi)$ from the nonlinear Eq. (3.2). The inverse problem is to determine $\lambda(\phi)$ or $\mu(\phi)$ from a knowledge of $\epsilon(\omega)$. This is most important for applications such as well logging. Particularly important is the problem of determining $\lambda(\phi)$ from $\epsilon(\omega)$ and $\mu(\phi)$ in view of the fact that the local porosity distribution $\mu(\phi)$ can be observed much more easily than the local percolation probabilities.

Consider therefore briefly the problem of determining $\lambda(\phi)$ from Eq. (3.2) given $\epsilon(\omega)$ and $\mu(\phi)$. A general theoretical discussion can be given based on the observation that Eq. (3.2) is now linear. It can be written as

$$\int_0^1 K(\omega;\phi)\lambda(\phi)d\phi = f(\omega) , \tag{7.1}$$

where

$$K(\omega;\phi)=\mu(\phi)\left[\frac{\epsilon_C(\omega;\phi)-\epsilon(\omega)}{\epsilon_C(\omega;\phi)+2\epsilon(\omega)}-\frac{\epsilon_B(\omega;\phi)-\epsilon(\omega)}{\epsilon_B(\omega;\phi)+2\epsilon(\omega)}\right] , \tag{7.2}$$

$$f(\omega)=-\int_0^1 \frac{\epsilon_B(\omega;\phi)-\epsilon(\omega)}{\epsilon_B(\omega;\phi)+2\epsilon(\omega)}\mu(\phi)d\phi . \tag{7.3}$$

Equation (7.1) is a linear Fredholm integral equation of the first kind. Because the kernel $K(\omega;\phi)$ is not symmetric, define

$$K_1(\omega,\omega')=\int_0^1 K(\omega,\phi)K(\omega',\phi)d\phi ,$$
$$K_2(\phi,\phi')=\int_0^1 K(\omega,\phi)K(\omega,\phi')d\omega .$$

General results can be employed to solve Eq. (7.1) if $f(\omega)$ is continuous and such that $\int_0^1 f(\omega)^2 d\omega$ exists, and if $\int_0^1\int_0^1 K_i(\omega;\phi)d\omega\, d\phi$ exists and $K_i(\omega;\phi)$ is piecewise continuous in $0\le\omega\le 1$, $0\le\phi\le 1$. The K_i are symmetric and have eigenvalues λ_n^2. The normal modes called Ω_{ni} and Φ_{ni} can be chosen orthonormal and satisfy

$$\lambda_n\int_0^1 K(\omega;\phi)\Omega_{ni}(\phi)d\phi=\Phi_{ni}(\omega) ,$$
$$\lambda_n\int_0^1 K(\omega;\phi)\Phi_{ni}(\omega)d\omega=\Omega_{ni}(\phi) .$$

These modes are used to solve Eq. (7.1). If (7.1) has any solution, then the inhomogeneity $f(\omega)$ can be written as

$$f(\omega)=\sum_{n,i}\Phi_{ni}(\omega)\int_0^1 f(\omega')\Phi_{ni}(\omega')d\omega' . \tag{7.4}$$

It is assumed that the two sets Ω_{ni} and Φ_{ni} have been made orthonormal. Then the solution to Eq. (7.1) is given as

$$\lambda(\phi)=\sum_{i,n}\lambda_n\Omega_{ni}(\phi)\int_0^1 f(\omega')\Phi_{ni}(\omega')d\omega' . \tag{7.5}$$

The eigenvalues λ_n^2 are the solutions of $D(\lambda^2)=0$, where

$$D(\lambda^2)=\sum_0^\infty \kappa_n\lambda^{2n} ,$$

$$\kappa_0=1,\quad K_i^{(0)}(x,y)=0 ,$$

$$\kappa_n=-\frac{1}{n}\int_0^1 K_i^{(n)}(x,x)dx ,$$

$$K_i^{(n)}(x,y)=\int_0^1 K_i(x,t)K_i^{(n-1)}(t,y)dt+\kappa_{n-1}K_i(x,y) .$$

These brief remarks about the inverse problem are intended to outline the general characteristics of the problem. A more detailed discussion must await the availability of experimentally observed local porosity distributions.[27]

VIII. CONCLUSION

Local porosity distributions and local percolation probabilities have been introduced as a partial geometric characterization of the complex pore-space geometry in porous media. From these well-defined and experimentally accessible geometric quantities, the dielectric response of general porous media resulting from geometrical disorder was calculated using simple effective-medium theory. It was found that the theory predicts an underlying percolation transition, which may or may not appear as a porosity threshold for conduction. As a consequence, percolation scaling theory can be applied to the case of porous media. This provides a theoretical framework inside which Archie's law can be understood as a statement about the diagenesis of rocks. In particular, the universal applicability of this phenomenological relationship appears as a consequence of the universality of the percolation transition. Simplest mean-field theory gives the value $m=2$ for the cementation exponent in the low-porosity limit. A new scaling law for the divergence of the real dielectric constant is predicted in the high-porosity limit. This law should be observable in conductor-filled insulating pore casts of systems obeying Archie's law. Numerical solutions for the effective dielectric constant show a surprising sensitivity to geometric details whenever the dispersion becomes large. The present theory contains no adjustable parameters or dis-

tribution functions. The dielectric response is calculated purely from geometrical quantities. Experimental observation of local porosity distributions and local percolation probabilities[27] must answer the question whether they are suitable geometric characteristics for distinguishing different classes of porous media or not.

ACKNOWLEDGMENTS

The author gratefully acknowledges financial support from the German-Norwegian research cooperation (Project B-2). He thanks Dr. B. Nøst for discussions and encouragement.

[1]J. R. Hearst and P. H. Nelson, *Well Logging for Physical Properties* (McGraw-Hill, New York, 1985).
[2]G. V. Keller and P. H. Licastro, U. S. Geol. Surv. Bull. **1052-H**, 257 (1959).
[3]G. V. Keller, in *Handbook of Physical Properties of Rock,* edited by R. S. Carmichael (CRC, Boca Raton, 1982), p. 217.
[4]J. Ph. Poley, J. J. Noteboom, and P. J. de Waal, Log. Anal. **19**, 8 (1978).
[5]W. E. Kenyon, J. Appl. Phys. **55**, 3153 (1984).
[6]G. E. Archie, Trans. Metall. Soc. AIME **146**, 54 (1942).
[7]I. Holwech and B. Nøst, Phys. Rev. B **39**, 12845 (1989).
[8]See also Ref. 5.
[9]See Ref. 13 for a review.
[10]D. Wilkinson, J. S. Langer, and P. N. Sen, Phys. Rev. B **28**, 1081 (1983).
[11]J. N. Roberts and L. M. Schwartz, Phys. Rev. B **31**, 5990 (1985).
[12]L. M. Schwartz and S. Kimminau, Geophysics **52**, 1402 (1987).
[13]P. N. Sen, C. Scala, and M. H. Cohen, Geophysics **46**, 781 (1981).
[14]P. N. Sen, Geophysics **46**, 1714 (1981).
[15]K. S. Mendelson and M. H. Cohen, Geophysics **47**, 257 (1982).
[16]P. N. Sen, Geophysics **49**, 586 (1984).
[17]P. Wong, J. Koplik, and J. P. Tomanic, Phys. Rev. B **30**, 6606 (1984).
[18]K. Ghosh and R. Fuchs, Phys. Rev. B **38**, 5222 (1988).
[19]D. Stroud, G. W. Milton, and B. R. De, Phys. Rev. B **34**, 5145 (1986).
[20]P. C. Lysne, Geophysics **48**, 775 (1983).
[21]J. Korringa, Geophysics **49**, 1760 (1984).
[22]R. Fuchs, Phys. Rev. B **11**, 1732 (1975).
[23]D. J. Bergman, Ann. Phys. (N.Y.) **138**, 78 (1982).
[24]A. E. Scheidegger, *The Physics of Flow through Porous Media* (University of Toronto Press, Toronto, 1974).
[25]F. A. L. Dullien, *Porous Media* (Academic, New York, 1979).
[26]C. D. Tsakiroglou and A. C. Payatakes, J. Colloid. Interface Sci. **137**, 315 (1990).
[27]Such observations are currently in progress both from simulations and from experiment
[28]M. Rovere, D. W. Heermann, and K. Binder, J. Phys. Cond. Matter **2**, 7009 (1990).
[29]D. A. G. Bruggeman, Ann. Phys. (Leipzig) **24**, 636 (1935).
[30]P. M. Kogut and J. P. Straley, J. Phys. C **12**, 2151 (1979).
[31]S. Alexander, J. Bernasconi, W. R. Schneider, and R. Orbach, Rev. Mod. Phys. **53**, 175 (1981).
[32]A. L. Efros and B. I. Shklovskii, Phys. Status Solidi B **76**, 475 (1976).
[33]D. Stroud and D. J. Bergman, Phys. Rev. B **25**, 2061 (1982).
[34]See R. Hilfer, Phys. Scr. (to be published) for a more general viewpoint.
[35]See, e.g., P. A. Scholle, AAPG Report No. 28, 1979 (unpublished), p. 181.